



# Effects of the Moisture Content on the Flow Behavior of Milled Woody Biomass

July 2023

*Changing the World's Energy Future*

Yimin Lu, Wencheng Jin, Jordan Lee Klinger, Sheng Dai



**DISCLAIMER**

This information was prepared as an account of work sponsored by an agency of the U.S. Government. Neither the U.S. Government nor any agency thereof, nor any of their employees, makes any warranty, expressed or implied, or assumes any legal liability or responsibility for the accuracy, completeness, or usefulness, of any information, apparatus, product, or process disclosed, or represents that its use would not infringe privately owned rights. References herein to any specific commercial product, process, or service by trade name, trade mark, manufacturer, or otherwise, does not necessarily constitute or imply its endorsement, recommendation, or favoring by the U.S. Government or any agency thereof. The views and opinions of authors expressed herein do not necessarily state or reflect those of the U.S. Government or any agency thereof.

# **Effects of the Moisture Content on the Flow Behavior of Milled Woody Biomass**

**Yimin Lu, Wencheng Jin, Jordan Lee Klinger, Sheng Dai**

**July 2023**

**Idaho National Laboratory  
Idaho Falls, Idaho 83415**

**<http://www.inl.gov>**

**Prepared for the  
U.S. Department of Energy  
Under DOE Idaho Operations Office  
Contract DE-AC07-05ID14517**

# Effects of the Moisture Content on the Flow Behavior of Milled Woody Biomass

Yimin Lu, Wencheng Jin,\* Jordan Lee Klinger, and Sheng Dai\*

Cite This: *ACS Sustainable Chem. Eng.* 2023, 11, 11482–11489

Read Online

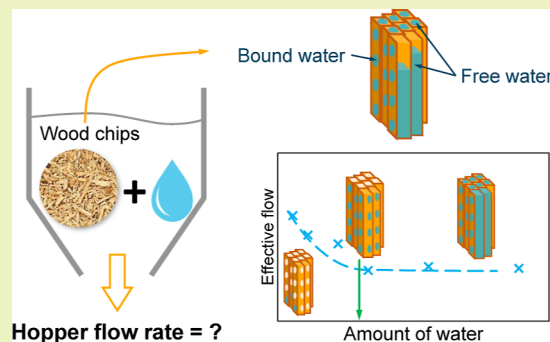
ACCESS |

Metrics &amp; More

Article Recommendations

**ABSTRACT:** Handling milled biomass particles in equipment like hoppers and feeders has been a long-lasting challenge in the bioenergy industry because of the poor flowability of these low density, high aspect ratio, and irregularly shaped particles. The inner pores of woody biomass particles complicate the granular flow behavior. When water exists in these intra- and inter-particle pores with sizes ranging from nanometers to micrometers, intricate processes such as hydrogen bonding, capillary effects, liquid bridge, and lubrication occur. However, knowledge of how these processes alter the bulk flow behavior of woody biomass particles is severely lacking. This study investigates the bulk flow behavior of loblolly pine chips in wedge-shaped hoppers considering moisture content. The fiber saturation point (FSP) of the material (30%) was determined through the differential scanning calorimetry analysis. The compressibility and shear resistance were found to increase with the increased moisture content through meso-scale testing. Moreover, hopper flow simulations suggest that the effective discharge rate decreases by 50% with the increasing moisture content up to the FSP, beyond which moisture content has no apparent influence on the effective discharge. This study highlights the importance of quantifying the biomass FSP in understanding biomass flowability at various moisture contents and sheds light on the trouble-free handling of wet woody biomass particles in the bioenergy industry.

**KEYWORDS:** granular mechanics, soft particles, particle swelling, particle rheology, material handling, renewable energy



## INTRODUCTION

Biomass to biofuel has become one of the most promising energy resources to replace fossil aviation fuels.<sup>1–4</sup> However, the economic competitiveness of the biofuel industry still suffers from the unstable flow and jamming of granular biomass materials in various feedstock handling equipment like hoppers and feeders.<sup>5–10</sup> Solving these issues centers on the fundamental understanding and accurate prediction of milled biomass's mechanical and rheological properties. Recent multi-scale experimental and numerical investigations promoted the knowledge of the flow behavior of dry or room-moisture woody biomass particles.<sup>11–14</sup> However, biorefineries often have to process wet materials with water from the original plants or due to outdoor transport and storage. Wet biomass materials usually have worse flowability than dry particles<sup>15–17</sup> due to particle swelling, softening, and capillarity. Understanding the effects of the moisture content on the flow behavior of milled biomass is critical to comprehensively evaluate the material flowability during feedstock handling.

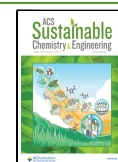
Current studies on the influence of the moisture content on biomass flowability include feeding and handling testing via hopper,<sup>11,12,15,18,19</sup> silo,<sup>16,17,20</sup> and screw feeder.<sup>21,22</sup> Laboratory characterizations of the moisture content influence on

material compressibility,<sup>12,15,23–28</sup> angle of repose (AoR),<sup>19,21,26,28,29</sup> shear responses,<sup>11,12,15,19,25–28,30–32</sup> and wall friction,<sup>23,24,28,31–33</sup> were also conducted. However, the link between the moisture-induced particle-scale and meso-scale property changes with macro-scale flow behavior has not been established for woody biomass. Previous investigations have mostly followed the Mohr–Coulomb framework,<sup>34</sup> which does not corroborate with experimental observations may be due to the limitations of the model or the methods to determine model parameters.<sup>15</sup> Recent studies, however, show that the Mohr–Coulomb framework is incapable of capturing the high compressibility, dilation, and history-dependent shear behavior of biomass particles<sup>13,35</sup> that have been observed in physical testings. Thus, it is necessary to apply the recently developed numerical framework<sup>36</sup> based on the Gudehus–Bauer (G–B) hypoplastic model, which can describe the flow

Received: March 6, 2023

Revised: July 14, 2023

Published: July 28, 2023



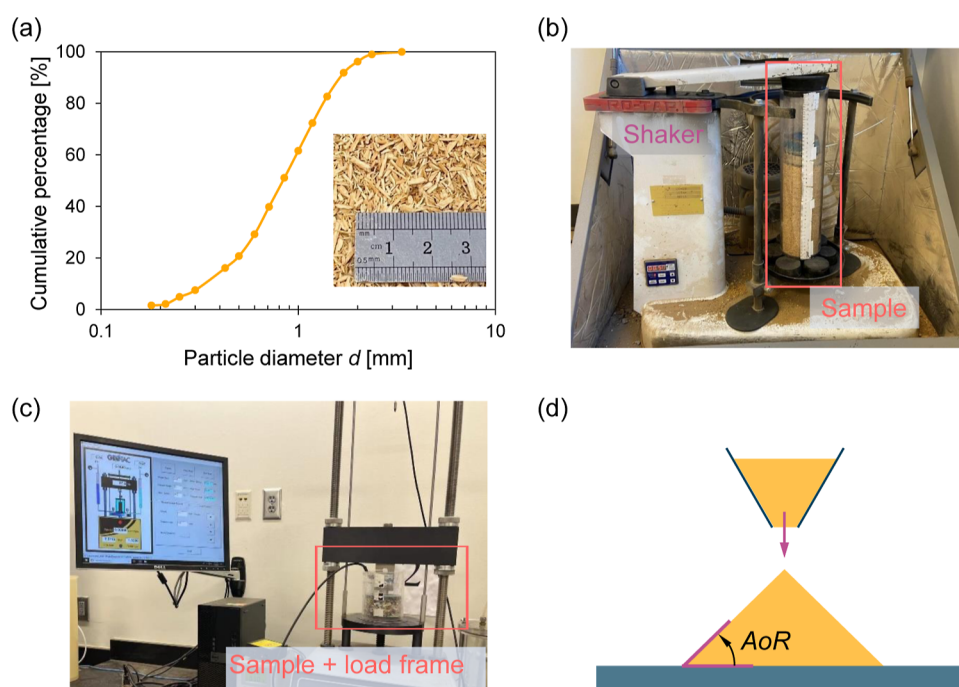


**Figure 1.** (a) Particle size distribution of the pine sample used in this study with the size and shape presented in the photograph. (b) Vibration test setup to measure the maximum density of the sample with varying loads. The setup consists of a shaker and the biomass sample placed in a cylinder with dead loads on the top. (c) Oedometer test setup to obtain the density–pressure response. (d) Schematic view of the AoR test with the funnel method.

behavior of woody biomass materials, to investigate the influences of the moisture content during feedstock handling. The G–B hypoplastic model incorporates the critical state theory, density dependency, and nonlinear elasticity, which are critical for accurately predicting flow features of milled biomass.<sup>14,37</sup>

In addition, milled woody biomass mostly has pores inside particles, and the pore size is often at the magnitude of nanometer to micrometer.<sup>38</sup> These internal micropores complicate biomass particle properties in the presence of water as multiple mechanisms may exist simultaneously, e.g., hydrogen bonding, capillary force, water-induced particle deformation, particle aggregates caused by surface tension, and water lubrication. Understanding how these mechanisms influence the flow behavior and identifying the range of moisture content dominating mechanical behaviors are greatly needed.

To address this knowledge gap, this study investigates the flow behavior of loblolly pine chips influenced by the moisture content with multi-scale experiments and numerical simulations. The thermogravimetric analysis (TGA) and the differential scanning calorimetry (DSC) test were performed to understand sample components and obtain the fiber saturation point (FSP) of the particles. Packing, oedometer, and AoR tests were conducted to investigate the compressibility and the shear behavior at bulk or laboratory scale. Moreover, by deploying an existing numerical framework to simulate hopper flow, the impacts of moisture on the flow behavior of wet woody biomass at the equipment scale are evaluated. The results highlight the importance of quantifying the biomass FSP to better assess its flow behavior at various moisture conditions.

## METHODS

**Biomass Sample.** The material used in this work is milled loblolly pine.<sup>13,36</sup> The original wood was hammer-milled until the particles could pass a 6 mm sieve, and then, the wood chips were dried in a rotary drum until the room moisture content was reached. The particle size distribution obtained from sieve analysis is presented in Figure 1a with a photo showing particle size and shape. Admittedly, sieve analysis tends to measure the smallest dimension of an elongated particle-like shredded pine here and thus is not an ideal method. However, the aspect ratio of these particles is typically around 1:6 to 1:10. The original moisture content of pine chips is 9.5% (dry basis) measured by the oven-drying method. During each test, the sample was first oven dried for 24 h, and then, a specific amount of water was added to and mixed uniformly with the dry particles to achieve the desired moisture content. The moisture content in this study is defined according to dry basis, i.e.

$$MC = \frac{m_w}{m_s} \times 100\% \quad (1)$$

where  $m_w$  and  $m_s$  stand for the mass of water and solids, respectively.

**Experimental Methods and Setups.** *Differential Scanning Calorimetry.* The DSC test was conducted with the TA DSC 250 to determine the FSP of pine chips. The DSC test measures the moisture content at which the cell walls are fully saturated with bound water, and no free water exists. Water was first added to the original pine samples until the moisture content was higher than the FSP, which can normally range from 10 to 50%.<sup>39</sup> Then, around 5 mg of the sample was placed in the DSC cell, heated from  $-20$  °C until  $20$  °C with a heating rate of  $2$  °C/min. During heating, the time-lapse temperature was measured, and the time-lapse heat flow was calculated by comparing the temperature difference between the sample and a reference point in the tester. The tests were conducted four times with different starting moisture contents (see the [Fiber Saturation Point](#) Section).

*Thermogravimetric Analysis.* TGA was performed using EXSTAR TG/DTA 7300 to understand the components of the pine sample. Around 7 g of the original sample (with room moisture content) was placed in the TGA cell and heated from room temperature (around

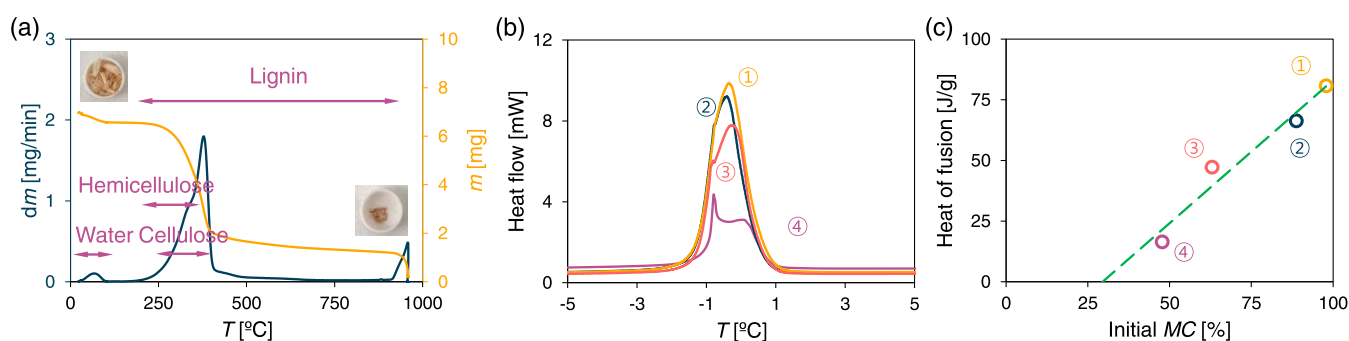


**Figure 2.** Particle characterization results. (a) Results from the TGA showing the evolution of mass and its derivative by raising the temperature. (b) Results from the DSC tests presenting the heat flow as a function of temperature. (c) Heat of fusion as a function of the initial moisture content computed from the DSC tests.

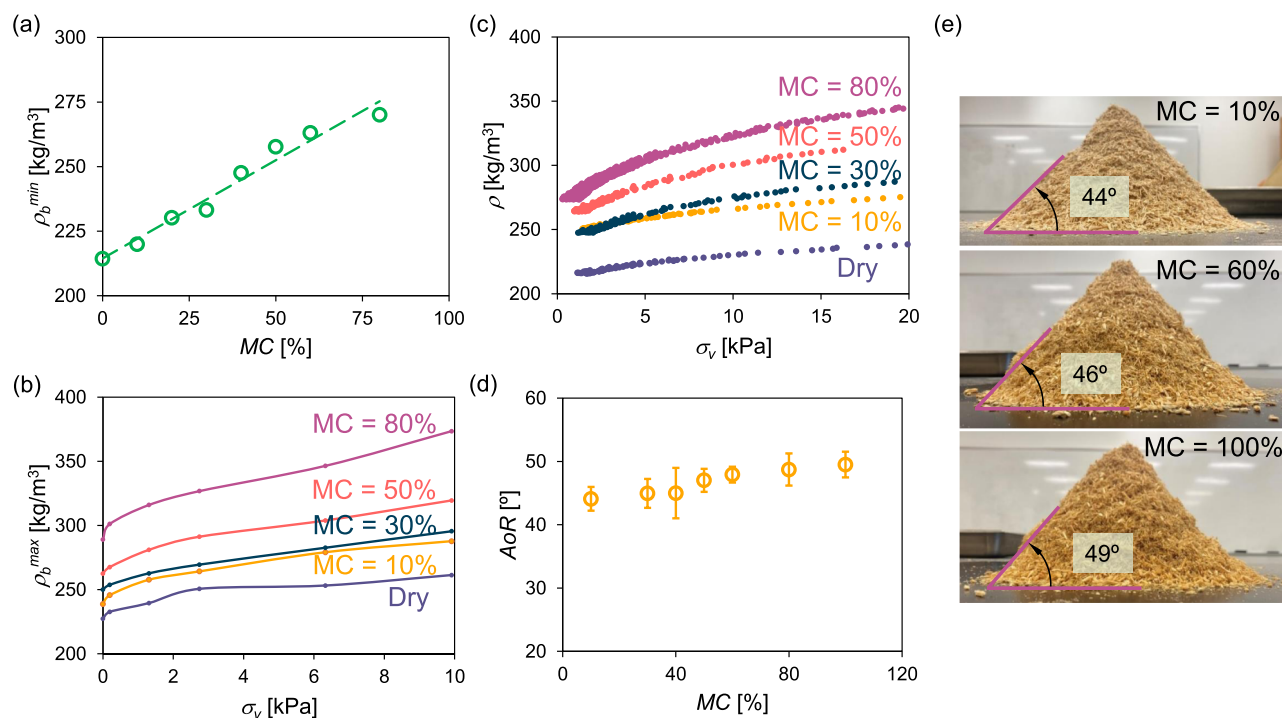


**Figure 3.** Experimental results demonstrating the material compressibility. (a) Minimum density  $\rho_b^{\min}$  as a function of the moisture content. (b) Maximum density  $\rho_b^{\max}$  determined after vibration at different surcharge loads and different moisture contents. (c) Bulk density changing with compressive pressure at different moisture contents determined from oedometer tests. (d) AoR determined by the funnel method as a function of the moisture content, where each point was averaged from 10 data points and the error bars represent the standard deviation. (e) Photographs of the repose angles at different moisture contents.

20 °C) to 950 °C with a heating rate of 20 °C/min in a nitrogen atmosphere (with a flow rate of 100 mL/min). Then, the sample was kept at 950 °C with air for 10 min followed by cooling back to room temperature. The temperature-dependent weight change and the rate of weight change were determined.

**Packing Density.** The density evolution with pressure was determined by the minimum/maximum (min/max) density tests according to the ASTM standards.<sup>40,41</sup> The minimum density was achieved by the “rainfall” method described in our previous work;<sup>36</sup> while the maximum density was obtained by vibrating the sample for 5 min with the W.S.Tyler Ro-tap RX-29 shaker (as shown in Figure 1b). The maximum density was determined with the pressure ranging from 0 to 10 kPa, which covers the pressure range in most of the bioenergy material handling applications.<sup>36</sup> The sample is placed in a cylindrical container with an inner diameter of 102 mm (Figure 1).

**Oedometer Test.** Continuous density–pressure relationships of the pine samples with various moisture contents were obtained from the oedometer tests. As shown in Figure 1c, samples were air-pluviated

into a 102 mm (4 in.) diameter oedometer cell, which was placed within a loading frame with displacement and load measurements. All samples were loaded until the vertical pressure exceeded 20 kPa, which can cover most of the bioenergy material handling applications, at a rate of 20% strain per hour.

**Angle of Repose.** AoR tests with a funnel<sup>42</sup> were conducted for the tested pine chips at different moisture contents. An illustration of the funnel method is presented in Figure 1d. The funnel has a diameter of 265 mm and an inclination angle of 40°. The mass of the sample was kept constant at 1.2 kg, and the dropping height was kept 15 cm above the top of the cone. The material was discharged through a 25.6 mm (1 in.) orifice, right after being deposited without a settlement. Materials flowing from the funnel deposit on a smooth-surface acrylic plate, forming a conical pile. The AoR was determined through image analysis of the taken photographs of the deposited piles. For each moisture content, at least 10 tests were repeated.

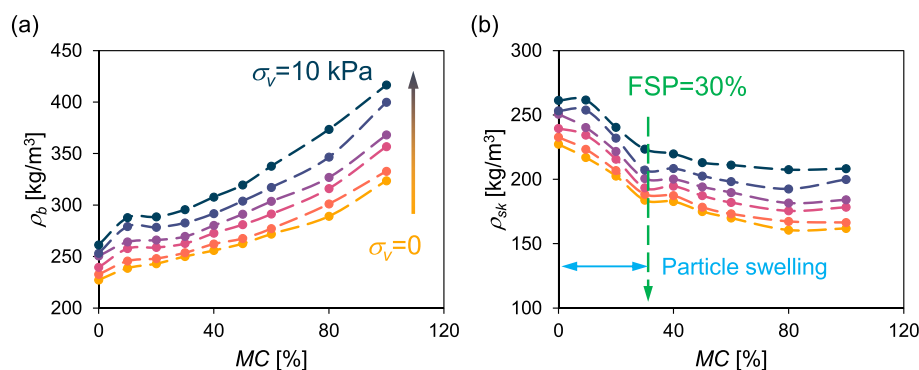


**Figure 4.** (a) Maximum bulk density of samples after vibration at different moisture contents, where the lines from bottom to the top represent applied compressive pressure from 0 to 10 kPa. (b) Particle skeleton density  $\rho_{sk}$ , defined as the bulk density of particle skeleton (solids), as a function of the moisture content.

## RESULTS

**Fiber Saturation Point.** The TGA results are presented in Figure 2a, where the orange line represents the mass of the specimen left on the pan with increasing temperature. The dark line is the changing rate of the mass, the dominant peak of which corresponds to cellulose and hemicellulose, whose major decomposition temperature range is 200–400 °C.<sup>43</sup> The decomposition temperature of lignin spans from 150 to 1000 °C. The final small peak stands for the mass burned in oxygen-rich gas (air). It can be determined that the pine chips tested in this study consist of 3% inorganic matter, 6% water, 65% cellulose and hemicellulose, and 26% lignin and other matters.

Presented in Figure 2b are the results from four DSC tests using samples with initial moisture contents of 48, 63, 89, and 98%. The water molecules in biomass particles can be generally categorized into two types: (1) bound water, which is physically adsorbed in cell walls and held by molecular forces at the hydroxyl sites of cellulose materials and (2) free water, which mainly resides in the lumen of cells or the outside of particles, and they can be easily driven off. Because the melting point of ice drops with increasing pressure, the bound water (ice) is usually hard to freeze (melt) because of the high pressure caused by the small channel size. When raising the temperature from −20 °C in each test, ice starts melting from molecules with higher pressure toward those with lower pressure, and the heat flow gradually increases correspondingly. Since the majority of molecules still have relatively low pressure, the melting and the heat flow reach the maximum when the temperature approaches zero, which is the melting point of ice at atmospheric pressure.

The FSP, defined as the moisture content at which the cell walls are saturated with bound water and no free water exists, was determined from DSC results by the extrapolation method:<sup>39,44,45</sup> (1) calculating the melting enthalpy  $\Delta H_m$  of samples with different initial moisture contents, (2) plotting the  $\Delta H_m$ – $MC_{init}$  data points, (3) extrapolating the line and obtaining the intersect with the  $MC_{init}$  axis, which stands for the moisture content at which the  $\Delta H_m = 0$ , i.e., the FSP. As shown in Figure 2c, the FSP of the tested material in this study is 30%.

**Compressibility.** Results of min/max density and oedometer tests of tested biomass particles with various moisture content are presented in Figure 3. Figure 3a shows that the minimum density  $\rho_b^{min}$  linearly increases with the increasing moisture content. The maximum density measured from the vibrating table tests is shown in Figure 3b, where each line

stands for the post-vibration density at vertical pressure from 0 to 10 kPa for different moisture contents. It can be seen that the bulk density increases with both applied stress and moisture content. In addition, the oedometer results in Figure 3c show that the sample compressibility, manifested as the range of density change caused by the same pressure increase, increases with the increased moisture content.

**Static Friction.** The AoR tests were conducted with the funnel method, and the results are presented in Figure 3d, with photographs demonstrating the AoR at different moisture contents in Figure 3e. The AoR of pine chips at room moisture content is around 44°, which is similar to the internal friction angle 47.3° determined with the combined experimental–numerical method described in the previous work.<sup>36</sup> Note that small variations of material parameters may exist due to the variability of biomass materials caused by the origin of the sample, i.e., different tree age, height, and the position and fraction of the tree.<sup>37,46,47</sup> The AoR generally increases with higher moisture content, which implies a higher shear (flow) resistance at a high moisture content. Particle breakage, which can influence the material internal friction and material-wall friction,<sup>48–50</sup> was not observed due to the low level of applied stress.

## ANALYSES AND DISCUSSION

**Particle Swelling.** Figure 4a shows that the bulk density of biomass samples subjected to each constant stress increases with the increasing moisture content. However, the “effective” density, i.e., the packing of the corresponding dry biomass skeleton, decreases with the increasing moisture content (Figure 3b). The effective skeleton density  $\rho_{sk}$  is defined as

$$\rho_{sk} = \rho_b \times \frac{1}{1 + MC} \quad (2)$$

which measures the density of the particle skeleton alone. The results in Figure 4b suggest that the biomass particles are compacted denser with less moisture before the FSP(30%), beyond which the moisture content has negligible impacts on the skeleton packing density. This is mainly because the molecular structures of cellulose and hemicellulose fibers shrink with water loss (i.e., biomass particles swell upon wetting) when the moisture content is below FSP. The moisture-induced particle swelling ceases after the cell walls are fully saturated by water (i.e., reaching the FSP).

In addition, we also noticed that particle aggregation occurred when the moisture content reached around 40 to

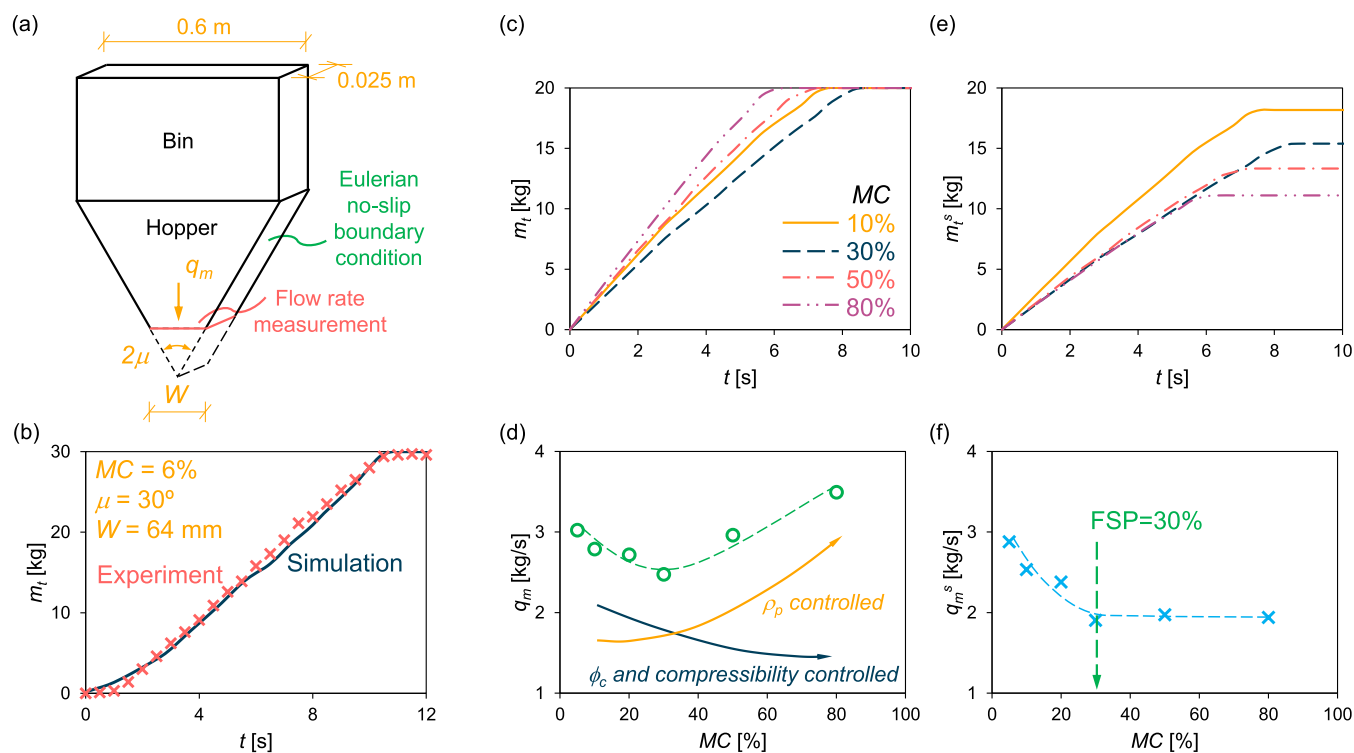


**Figure 5.** Numerical modeling, validation, and results. (a) Geometry and boundary conditions for the numerical hopper flow model, which simulates a slice of the hopper-bin system according to the plane-strain condition. (b) Validation of the numerical modeling by the comparison of the numerical flow response (time-lapse cumulative discharged mass  $m_t$  plotted as the line) against the experimental measurements (“x”s). (c) Time-lapse discharged mass  $m_t$  at different moisture contents, where the slope stands for the mass flow rate  $q_m$ , and  $q_m$  is plotted in (d) against the moisture content. (e) Effective discharged mass,  $m_t^s$ , defined as the discharged total mass of solid (with the water removed), changing with time. The effective mass flow rate  $q_m^s$  is plotted in (f) against the moisture content.

60% during the tests. This aggregation of small particles can be attributed to the capillarity when a small amount of free water resides at the inter-particle contacts.

**Flow Behavior in Wedge-Shaped Hoppers. Numerical Modeling.** To evaluate the influence of the moisture content on the flow behavior at the equipment scale, hopper simulations were conducted, and the flow rates at different moisture contents were extracted and compared. To address the mesh tangling issue of FEM when simulating large deformation, the coupled Eulerian–Lagrangian FEM scheme<sup>36,37</sup> was applied, which was realized by two steps: a deformation step, where the material deformed with the mesh, followed by a remapping step, where the deformed mesh was returned to its original position and the material (deformed) properties were interpolated back to the “fixed” mesh. A quasi-3D model, i.e., a 2D plane-strain slice of the wedge-shaped hopper, was developed and presented in Figure 5a. The numerical model is the same as the one developed in the previous work<sup>14,37</sup> except for the boundary conditions on hopper walls. In this study, the no-slip boundary was implemented on both hopper walls by directly fixing all six degrees of freedom of boundary nodes. Given the magnitude of the hopper wall friction has trivial influences on the flow rate,<sup>14,36</sup> this Eulerian boundary condition will not undermine the prediction accuracy of the hopper flow rate. In addition, no Eulerian–Lagrangian contacts can boost the computational efficiency.

Among various constitutive models simulating the flow behavior of milled biomass,<sup>35</sup> the Gudehus–Bauer (G–B) hypoplastic model<sup>51,52</sup> has been implemented and utilized to

explore the physics of biomass granular flow with success.<sup>14,36,37,53</sup> Therefore, the G–B model is also used in this study to simulate biomass flow behavior with various moisture contents. The G–B hypoplastic model describes the Jaumann stress rate  $\dot{\sigma}$  as a function of the current state (i.e., stress  $\sigma$  and void ratio  $e$ ) for a given strain rate  $\dot{\gamma}$ . Treating void ratio as one of the state variables enables the model capable of capturing high compressibility of biomass materials

$$\begin{aligned}\dot{\sigma} &= f(\sigma, \dot{\gamma}, e) = f_s(\mathbb{L}: \dot{\gamma} + f_d N \sqrt{\dot{\gamma}}: \dot{\gamma}) \\ \dot{e} &= (1 + e)\text{tr}(\dot{\gamma})\end{aligned}\quad (3)$$

where coefficients  $f_s$  and  $f_d$  are the combination of pyknropy and barotropy factors, which consider the influence of the void ratio and pressure level on the stress and shear strength and enforce the state variables satisfy the critical state condition.<sup>51,52</sup>  $\mathbb{L}$  and  $N$  are the elastic and plastic modulus expressed as the forth- and second-order tensor functions of current state, this formulation makes the model capable of modeling nonlinear behavior at each increment. All these features are important to capture the flow behavior of milled biomass.<sup>36</sup>

The hypoplastic model parameters can be divided into three categories: (1) the minimum, critical state, and maximum void ratio at zero pressure  $e_{d0}$ ,  $e_{c0}$ , and  $e_{i0}$ , (2) compressibility-related parameters  $h_s$ ,  $n$ , and  $\beta$ , and (3) shear-related parameters  $\phi_c$  and  $\alpha$ . Detailed description and calibration of these parameters and the G–B hypoplastic model formulation were reported in the previous work.<sup>36</sup> In this study, the hypoplastic material parameters were calibrated from the min/

Table 1. Calibrated G–B-Hypoplastic Model Parameters of Pine Chips at Different Moisture Contents

MC (%)	$\rho_p$ [kg/m <sup>3</sup> ]	$\phi_c$ [deg]	$h_s$ [kPa]	$n$ [—]	$e_{d0}$ [—]	$e_{c0}$ [—]	$e_{i0}$ [—]	$\alpha$ [—]	$\beta$ [—]
5	410.5	43.63	214.6	0.43	0.73	0.91	1.08	0.15	1.63
10	430.0	44.09	230.5	0.48	0.78	0.95	1.05	0.10	0.50
20	469.1	44.66	171.0	0.43	0.88	1.05	1.26	0.20	1.00
30	508.2	44.96	138.6	0.38	0.99	1.14	1.59	0.20	2.00
50	586.4	47.02	119.7	0.39	1.19	1.32	1.84	0.20	2.00
80	703.6	48.72	90.1	0.45	1.50	1.59	2.22	0.10	2.00

max density (Packing Density Section), oedometer (Oedometer Test Section), the AoR tests (Angle of Repose Section), and single-element FEM simulations following a similar procedure reported by Lu et al.<sup>36</sup> except that (1) the critical state friction angle  $\phi_c$  was determined by AoR tests and (2)  $\alpha$ ,  $\beta$ , and  $e_{i0}$  were determined by single-element FEM simulations of the oedometer tests. The calibrated parameters are listed in Table 1. Note that the parameters of 10, 30, 50, and 80% moisture content were calibrated from the aforementioned procedure, while that of 5 and 20% were interpolated/extrapolated. A few assumptions were made during the calibration: (1) particle density  $\rho_p$  was estimated by assuming fixed particle volume and (2) free water can reside within the particle's inner pores or outside particles. The latter may induce capillarity, which cannot be explicitly captured by the continuum-based model, but its impacts to flow behavior have been reflected via measured parameter values. Admittedly, the current model does not capture moisture content explicitly, but its impacts on biomass flow behavior are reflected by the changes in material properties listed in Table 1. Thus, for a given arbitrary moisture content, one can interpolate the parameters based on Table 1, but a new constitutive model capturing moisture content explicitly is needed.

The hypoplastic parameters in Table 1 reflect the evolution of the physical properties of biomass particles due to the moisture content change. As the moisture content increases, the water starts to move into particles, making the particle density increase. The friction angle slightly increases manifested in the AoR tests. The granulate hardness  $h_s$  decreases, indicating the increase in compressibility. The large increase of the extreme void ratios ( $e_{d0}$ ,  $e_{c0}$ , and  $e_{i0}$ ) used for modeling is mainly caused by the assumptions mentioned above and does not imply a physical increase.

The modeling predicted flow response, i.e., the cumulative discharged mass against time, was obtained by integrating bulk density and velocity across all elements of the outlet surface and time. The predicted flow response was then used to validate the numerical model against the physical hopper flow experiment.<sup>14,37</sup> As demonstrated in Figure 5b, the numerical prediction (the line) agrees well with experimental measurements (the "x"s) at MC = 6%.

**Hopper Flow Affected by the Moisture Content.** Hopper flow simulations were conducted with a fixed hopper geometry (inclination angle  $\mu = 45^\circ$ , outlet width  $W = 60$  mm), the same packing condition [i.e., the initial void ratio  $e_{init} = 1/2(e_{d0} + e_{c0})$ , which represents a relatively loose packing], and the same initial weight of material  $M$ . The predicted mass flow rates are presented in Figure 5.

Figure 5c plots the time-lapse total discharged mass  $m_t$  for pine chips with the moisture content varying from 10 to 80%, where the slope measures the mass flow rate  $q_m$ . Figure 5d shows that the mass flow rate  $q_m$  first decreases and then

increases with the increased moisture content. The results highlight that two competing mechanisms govern the physical process of hopper discharge of wet biomass particles: (1) increased moisture content increases the shear/flow resistance manifested as the increasing AoR and compressibility of the material and (2) adding water into the sample increases the self-weight which facilitates the flow via increasing driven force by gravity. As illustrated in Figure 5d, the increased shear resistance and compressibility govern the flow behavior when the moisture content is small (before reaching the FSP), while the increased discharge-driven force governs the flow behavior when the moisture content is large. The lowest rate of total discharge is encountered at an intermediate moisture content.

As mentioned in Particle Swelling section, particle aggregation was observed when mixing biomass particles with water, indicating the existence of cohesion. The G–B hypoplastic model used in this study cannot capture the cohesion behavior, which may underestimate the flow resistance with intermediate and high moisture contents. Therefore, the flow rate for wet biomass with intermediate and high moisture content should be lower than what has been predicted here. An advanced constitutive model is in development to capture the flow behavior of wet biomass particles.

To evaluate the discharge of biomass solids only (i.e., excluding the discharged water), the effective discharged mass  $m_t^s$  is defined here as the total discharged mass minus the discharged water and can be calculated by

$$m_t^s = m_t \times \frac{1}{1 + MC} \quad (4)$$

The time-lapse response of the effective discharged mass  $m_t^s$  is presented in Figure 5e, with the corresponding effective mass flow rate  $q_m^s$  plotted in Figure 5f. The results clearly show that with the increasing moisture content, the effective mass flow rate decreases 50% until reaching the FSP, after which the effective mass flow rate stays constant. Therefore, the reduced moisture content particularly below FPS in milled woody biomass promotes the hopper discharge efficiency for biomass solids.

## CONCLUSIONS

This work quantifies the FSP of milled woody biomass particles and ensued changes in its various fundamental physical and mechanical properties with varying moisture conditions. By deploying an existing numerical framework, the impacts of moisture on the bulk flow of woody biomass particles through industry-scale hoppers are evaluated. Salient conclusions are as follows:

- The FSP of tested loblolly pine chips is 30% using the DSC method. Milled pine particles swell with the increased moisture content until the FSP is reached

(MC < FSP), beyond which the swelling ceases and becomes independent of the moisture content.

- Increased moisture content in pine chips leads to higher particle compressibility and increased AoR. Particle aggregation at a moisture content of 40–60% was observed due to capillarity from small amounts of free water residing at particle contacts.
- The flow behavior of wet biomass particles in hoppers is governed by two competing forces with the increased moisture content: increased internal friction that suppresses the flow and increased bulk density that accelerates the gravity-induced flow. The minimum discharge rate of the total mass occurs at a moisture content close to the FSP.
- For a given hopper configuration, the effective biomass flux, i.e., the discharge of biomass solids, excluding the discharged water from the bulk flow, decreases 50% with the increased moisture content until reaching the FSP. Therefore, decreasing the moisture content, particularly below its FSP, can greatly promote the effective discharge of biomass solids.
- The results in this study also highlight the necessity of quantifying the FSP of biomass to better understand and explain the impacts of the moisture content on various fundamental physical properties and macro-scale flow behaviors of biomass.

This study promotes the scientific understanding of the flowability of wet biomass particles and sheds light on the efficient handling of milled woody biomass with moisture.

## AUTHOR INFORMATION

### Corresponding Authors

**Wencheng Jin** – Energy and Environment Science & Technology Directorate, Idaho National Laboratory, Idaho Falls, Idaho 83415, United States; [orcid.org/0000-0002-2602-5068](https://orcid.org/0000-0002-2602-5068); Email: [wencheng.jin@inl.gov](mailto:wencheng.jin@inl.gov)

**Sheng Dai** – School of Civil and Environmental Engineering, Georgia Institute of Technology, Atlanta, Georgia 30332, United States; [orcid.org/0000-0003-0221-3993](https://orcid.org/0000-0003-0221-3993); Email: [sheng.dai@ce.gatech.edu](mailto:sheng.dai@ce.gatech.edu)

### Authors

**Yimin Lu** – School of Civil and Environmental Engineering, Georgia Institute of Technology, Atlanta, Georgia 30332, United States; [orcid.org/0000-0001-6022-2551](https://orcid.org/0000-0001-6022-2551)

**Jordan Lee Klinger** – Energy and Environment Science & Technology Directorate, Idaho National Laboratory, Idaho Falls, Idaho 83415, United States

Complete contact information is available at:  
<https://pubs.acs.org/10.1021/acssuschemeng.3c01344>

### Notes

The authors declare no competing financial interest.

## ACKNOWLEDGMENTS

This work was performed as part of the Feedstock Conversion Interface Consortium (FCIC) with funding provided by the U.S. Department of Energy Bioenergy Technologies Office. This article was authored by Idaho National Laboratory (managed by Battelle Energy Alliance) under contract no. DE-AC07-05ID14517 and by Georgia Institute of Technology through a subcontract. The views expressed in the article do

not necessarily represent the views of the DOE or the U.S. Government. The U.S. Government retains and the publisher, by accepting the article for publication, acknowledges that the U.S. Government retains a nonexclusive, paid-up, irrevocable, worldwide license to publish or reproduce the published form of this work, or allow others to do so, for U.S. Government purposes.

## REFERENCES

- (1) O'Connell, A.; Kousoulidou, M.; Lonza, L.; Weindorf, W. Considerations on GHG emissions and energy balances of promising aviation biofuel pathways. *Renewable Sustainable Energy Rev.* **2019**, *101*, 504–515.
- (2) Ng, K. S.; Farooq, D.; Yang, A. Global biorenewable development strategies for sustainable aviation fuel production. *Renewable Sustainable Energy Rev.* **2021**, *150*, 111502.
- (3) Prussi, M.; Lee, U.; Wang, M.; Malina, R.; Valin, H.; Taheripour, F.; Velarde, C.; Staples, M. D.; Lonza, L.; Hileman, J. I. CORSIA: The first internationally adopted approach to calculate life-cycle GHG emissions for aviation fuels. *Renewable Sustainable Energy Rev.* **2021**, *150*, 111398.
- (4) Holladay, J.; Abdullah, Z.; Heyne, J. *Sustainable Aviation Fuel: Review of Technical pathways*, 2020. DOI: [10.2172/1660415](https://doi.org/10.2172/1660415).
- (5) Miccio, F.; Barletta, D.; Poletto, M. Flow properties and arching behavior of biomass particulate solids. *Powder Technol.* **2013**, *235*, 312–321.
- (6) Falk, J.; Berry, R. J.; Broström, M.; Larsson, S. H. Mass flow and variability in screw feeding of biomass powders—Relations to particle and bulk properties. *Powder Technol.* **2015**, *276*, 80–88.
- (7) Ilic, D.; Williams, K.; Farnish, R.; Webb, E.; Liu, G. On the challenges facing the handling of solid biomass feedstocks. *Biofuels, Bioprod. Biorefin.* **2018**, *12*, 187–202.
- (8) Hess, J. R.; Wright, C. T.; Kenney, K. L. Cellulosic biomass feedstocks and logistics for ethanol production. *Biofuels, Bioprod. Biorefin.* **2007**, *1*, 181–190.
- (9) Dale, B. A sober view of the difficulties in scaling cellulosic biofuels. *Biofuels, Bioprod. Biorefin.* **2017**, *11*, 5–7.
- (10) Barletta, D.; Poletto, M. An assessment on silo design procedures for granular woody biomass. *Chem. Eng. Trans.* **2013**, *32*, 2209.
- (11) Klinger, J.; Saha, N.; Bhattacharjee, T.; Carilli, S.; Jin, W.; Xia, Y.; Daniel, R.; Burns, C.; Ajayi, O.; Cheng, Z.; et al. Multiscale Shear Properties and Flow Performance of Milled Woody Biomass. *Front. Energy Res.* **2022**, *10*, 855289.
- (12) Saha, N.; Goates, C.; Hernandez, S.; Jin, W.; Westover, T.; Klinger, J. Characterization of particle size and moisture content effects on mechanical and feeding behavior of milled corn (*Zea mays* L.) stover. *Powder Technol.* **2022**, *405*, 117535.
- (13) Jin, W.; Klinger, J. L.; Westover, T. L.; Huang, H. A density dependent Drucker-Prager/Cap model for ring shear simulation of ground loblolly pine. *Powder Technol.* **2020**, *368*, 45–58.
- (14) Lu, Y.; Jin, W.; Saha, N.; Klinger, J. L.; Xia, Y.; Dai, S. Wedge-Shaped Hopper Design for Milled Woody Biomass Flow. *ACS Sustainable Chem. Eng.* **2022**, *10*, 16803–16813.
- (15) Hernandez, S.; Westover, T. L.; Matthews, A. C.; Ryan, J. C. B.; Williams, C. L. Feeding properties and behavior of hammer-and knife-milled pine. *Powder Technol.* **2017**, *320*, 191–201.
- (16) Jensen, P. D.; Mattsson, J. E.; Kofman, P. D.; Klausner, A. Tendency of wood fuels from whole trees, logging residues and roundwood to bridge over openings. *Biomass Bioenergy* **2004**, *26*, 107–113.
- (17) Mattsson, J. E.; Kofman, P. D. Influence of particle size and moisture content on tendency to bridge in biofuels made from willow shoots. *Biomass Bioenergy* **2003**, *24*, 429–435.
- (18) Paulrud, S.; Mattsson, J. E.; Nilsson, C. Particle and handling characteristics of wood fuel powder: effects of different mills. *Fuel Process. Technol.* **2002**, *76*, 23–39.

- (19) Salehi, H.; Poletto, M.; Barletta, D.; Larsson, S. H. Predicting the silo discharge behavior of wood chips—A choice of method. *Biomass Bioenergy* **2019**, *120*, 211–218.
- (20) Mattsson, J. E.; Kofman, P. D. Method and apparatus for measuring the tendency of solid biofuels to bridge over openings. *Biomass Bioenergy* **2002**, *22*, 179–185.
- (21) Miao, Z.; Grift, T. E.; Hansen, A. C.; Ting, K. C. Flow performance of ground biomass in a commercial auger. *Powder Technol.* **2014**, *267*, 354–361.
- (22) Zareiforush, H.; Komarizadeh, M. H.; Alizadeh, M. R.; Masoomi, M. Screw conveyors power and throughput analysis during horizontal handling of paddy grains. *J. Agric. Sci.* **2010**, *2*, 147.
- (23) Crawford, N. C.; Nagle, N.; Sievers, D. A.; Stickel, J. J. The effects of physical and chemical preprocessing on the flowability of corn stover. *Biomass Bioenergy* **2016**, *85*, 126–134.
- (24) Mani, S.; Tabil, L. G.; Sokhansanj, S.; Roberge, M. Mechanical properties of corn stover grind. *2003 ASAE Annual Meeting*, 2003; p 1.
- (25) Stasiak, M.; Molenda, M.; Bańda, M.; Wiacek, J.; Parafiniuk, P.; Lisowski, A.; Gancarz, M.; Gondek, E. Mechanical characteristics of pine biomass of different sizes and shapes. *Eur. J. Wood Wood Prod.* **2019**, *77*, 593–608.
- (26) Littlefield, B.; Fasina, O.; Shaw, J.; Adhikari, S.; Via, B. Physical and flow properties of pecan shells—Particle size and moisture effects. *Powder Technol.* **2011**, *212*, 173–180.
- (27) Stasiak, M.; Molenda, M.; Bańda, M.; Gondek, E. Mechanical properties of sawdust and woodchips. *Fuel* **2015**, *159*, 900–908.
- (28) Wu, M.; Schott, D.; Lodewijks, G. Physical properties of solid biomass. *Biomass Bioenergy* **2011**, *35*, 2093–2105.
- (29) Ilejki, K.; Zhou, B. The angle of repose of bulk corn stover particles. *Powder Technol.* **2008**, *187*, 110–118.
- (30) Stasiak, M.; Molenda, M.; Gancarz, M.; Wiacek, J.; Parafiniuk, P.; Lisowski, A. Characterization of shear behaviour in consolidated granular biomass. *Powder Technol.* **2018**, *327*, 120–127.
- (31) Gil, M.; Schott, D.; Arauzo, I.; Teruel, E. Handling behavior of two milled biomass: SRF poplar and corn stover. *Fuel Process. Technol.* **2013**, *112*, 76–85.
- (32) Barletta, D.; Berry, R. J.; Larsson, S. H.; Lestander, T. A.; Poletto, M.; Ramírez-Gómez, A. Assessment on bulk solids best practice techniques for flow characterization and storage/handling equipment design for biomass materials of different classes. *Fuel Process. Technol.* **2015**, *138*, 540–554.
- (33) Larsson, S. H. Kinematic wall friction properties of reed canary grass powder at high and low normal stresses. *Powder Technol.* **2010**, *198*, 108–113.
- (34) Jenike, A. W. *Storage and Flow of Solids*; Bulletin of the University of Utah, 1964; Vol. 53.
- (35) Jin, W.; Stickel, J. J.; Xia, Y.; Klinger, J. A review of computational models for the flow of milled biomass Part II: Continuum-mechanics models. *ACS Sustainable Chem. Eng.* **2020**, *8*, 6157–6172.
- (36) Lu, Y.; Jin, W.; Klinger, J.; Westover, T. L.; Dai, S. Flow characterization of compressible biomass particles using multiscale experiments and a hypoplastic model. *Powder Technol.* **2021**, *383*, 396–409.
- (37) Lu, Y.; Jin, W.; Klinger, J.; Dai, S. Flow and arching of biomass particles in wedge-shaped hoppers. *ACS Sustainable Chem. Eng.* **2021**, *9*, 15303–15314.
- (38) Ciesielski, P. N.; Crowley, M. F.; Nimlos, M. R.; Sanders, A. W.; Wiggins, G. M.; Robichaud, D.; Donohoe, B. S.; Foust, T. D. Biomass particle models with realistic morphology and resolved microstructure for simulations of intraparticle transport phenomena. *Energy Fuels* **2015**, *29*, 242–254.
- (39) Passarini, L.; Zelinka, S. L.; Glass, S. V.; Hunt, C. G. Effect of weight percent gain and experimental method on fiber saturation point of acetylated wood determined by differential scanning calorimetry. *Wood Sci. Technol.* **2017**, *51*, 1291–1305.
- (40) ASTM Standard D4253-16, *Standard Test Methods for Maximum Index Density and Unit Weight of Soils Using a Vibratory Table*. DOI: 10.1520/D4253-16E01.
- (41) ASTM Standard D4254-16, *Standard test methods for minimum index density and unit weight of soils and calculation of relative density*. DOI: 10.1520/D4254-16.
- (42) Rousé, P. C. Comparison of methods for the measurement of the angle of repose of granular materials. *Geotech. Test. J.* **2014**, *37*, 20120144.
- (43) Díez, D.; Uruña, A.; Piñero, R.; Barrio, A.; Tamminen, T. Determination of hemicellulose, cellulose, and lignin content in different types of biomasses by thermogravimetric analysis and pseudocomponent kinetic model (TGA-PKM method). *Processes* **2020**, *8*, 1048.
- (44) Simpson, L. A.; Barton, A. F. M. Determination of the fibre saturation point in whole wood using differential scanning calorimetry. *Wood Sci. Technol.* **1991**, *25*, 301–308.
- (45) Zelinka, S. L.; Lambrecht, M. J.; Glass, S. V.; Wiedenhoef, A. C.; Yelle, D. J. Examination of water phase transitions in Loblolly pine and cell wall components by differential scanning calorimetry. *Thermochim. Acta* **2012**, *533*, 39–45.
- (46) Jordan, L.; Clark, A.; Schimleck, L. R.; Hall, D. B.; Daniels, R. F. Regional variation in wood specific gravity of planted loblolly pine in the United States. *Can. J. For. Res.* **2008**, *38*, 698–710.
- (47) Schultz, R. P. *Loblolly Pine: The Ecology and Culture of the Loblolly Pine (Pinus Taeda L.)*; US Government Printing Office, 1997; pp 26–27.
- (48) Wang, P.; Yin, Z.-Y. Effect of particle breakage on the behavior of soil-structure interface under constant normal stiffness condition with DEM. *Comput. Geotech.* **2022**, *147*, 104766.
- (49) Wang, P.; Yin, Z.-Y.; Wang, Z.-Y. Micromechanical investigation of particle-size effect of granular materials in biaxial test with the role of particle breakage. *J. Eng. Mech.* **2022**, *148*, 04021133.
- (50) Yin, Z.-Y.; Wang, P.; Zhang, F. Effect of particle shape on the progressive failure of shield tunnel face in granular soils by coupled FDM-DEM method. *Tunn. Undergr. Space Technol.* **2020**, *100*, 103394.
- (51) Gudehus, G. A comprehensive constitutive equation for granular materials. *Soils Found.* **1996**, *36*, 1–12.
- (52) Bauer, E. Calibration of a comprehensive hypoplastic model for granular materials. *Soils Found.* **1996**, *36*, 13–26.
- (53) Jin, W.; Lu, Y.; Chen, F.; Hamed, A.; Saha, N.; Klinger, J.; Dai, S.; Chen, Q.; Xia, Y. On the Fidelity of Computational Models for the Flow of Milled Loblolly Pine: A Benchmark Study on Continuum-Mechanics Models and Discrete-Particle Models. *Front. Energy Res.* **2022**, *10*, 855848.